



Efficiency improvement of a vector-controlled dual star induction machine drive system

Mokhtar Nesri¹ · Kamal Nounou¹ · Khoudir Marouani¹ · Azeddine Houari² · Mohamed Fouad Benkhoris²

Received: 1 February 2019 / Accepted: 9 January 2020 / Published online: 27 January 2020
© Springer-Verlag GmbH Germany, part of Springer Nature 2020

Abstract

This paper proposes an optimal vector control strategy to minimize copper losses and to improve the power factor and the efficiency of a multiphase induction machine drive system. Indeed, the proposed approach aims to minimize the magnetizing energy by adjusting the magnetic state of the motor regarding the drive's operating point. As a result, the current circulating through the motor windings can be reduced, which leads to copper losses reduction. Hence, an improvement in the machine's power factor and efficiency is obtained. Simulation and experimental results are carried out on a drive system based on a dual star induction machine to validate the proposed control approach.

Keywords Dual star induction machine (DSIM) · Vector control · Optimal flux · Joule losses · Power factor

1 Introduction

Recently, lots of researches have been conducted on multiphase electrical machines for both renewable energy and electromechanical energy conversion applications [1–4]. Indeed, increasing the number of phases offers additional degrees of freedom which enhance the power system reliability and the energy conversion quality. Such enhancement is widely testified and established in power segmentation, torque ripple reduction and fault-tolerant capability [1, 5–7].

Also, as most of the drive systems are devoted to variable speed as well as variable load operations, the total efficiency of such systems is affected by varying the operating

point [8]. Nowadays, several optimization techniques are introduced to enhance the variable speed drive efficiency [4, 9–12]. Likewise, the proposed control strategy presented in this paper tracks the operating point of the drive system to ensure that the operating conditions are optimal. So, the target of the control approach is to reduce the magnetizing energy, by adjusting the motor's magnetic state with respect to the operating point of the drive system. Accordingly, the current circulating through the windings of the motor can be clearly reduced, leading to Joule losses reduction and therefore to machine efficiency improvement. The control method is tested and verified on a DSIM drive system.

The proposed control approach is based on the principle of flux-oriented control (FOC), which has a simple structure and is widely employed in industrial processes. Generally, the FOC ensures that the magnitude of the motor's magnetizing flux is constant and equal to its nominal value. Consequently, optimal operation can be reached at the nominal operating point. Below that point, the efficiency of the drive system is reduced due to the excessive energy stored unnecessarily in the motor windings. Hence, the excessive stored energy can be reduced by adjusting the magnetizing flux according to the drive's operating point.

This paper is organized as follows. Sections 2 and 3 present the drive system and its model. In Sections 4 and 5, the proposed control technique is introduced and detailed. Sections 6, 7 and 8 exhibit the main simulation and experimental results carried out to validate the proposed strategy.

✉ Mokhtar Nesri
nesri_m@yahoo.fr

Kamal Nounou
nounou.kamal18@gmail.com

Khoudir Marouani
marouani_khoudir@yahoo.fr

Azeddine Houari
Azeddine.Houari@univ-nantes.fr

Mohamed Fouad Benkhoris
mohamed-fouad.benkhoris@univ-nantes.fr

¹ Ecole Militaire Polytechnique, LSEE UER-ELT,
16046 Bordj El-Bahri, Algiers, Algeria

² IREENA Laboratory, Université de Nantes, Nantes, France

2 Drive system description

The drive system studied in this work is based on a DSIM, where two symmetrical and identical sets of three-phase windings share a common stator magnetic core and are phase shifted spatially by 30° (electrical degrees) as depicted in Fig. 1. A voltage source inverter (VSI) is used to feed each set of the stator winding. The rotor of the DSIM is identical to that of the three-phase squirrel cage induction machine. Furthermore, the DSIM is considered as the combination of two three-phase machines sharing the same magnetic core. Hence, the usual Park transformation can be applied to each stator set [8, 13, 14].

3 Drive system modeling

Using the vector space decomposition approach introduced in [15], the original six-phase dimensional system can be decomposed into two main sub-models named (sd₁, sq₁) and (sd₂, sq₂) for the stator side and (rd, rq) for the rotor side, respectively [16]. The equations of the voltage and the flux are expressed in the following [8, 13, 14].

The sub-model of the stator voltage (sd₁–sq₁) is expressed as:

$$\begin{cases} V_{sd_1} = R_s I_{sd_1} + \frac{d\phi_{sd_1}}{dt} - \omega_s \phi_{sq_1} \\ V_{sq_1} = R_s I_{sq_1} + \frac{d\phi_{sq_1}}{dt} + \omega_s \phi_{sd_1} \end{cases} \quad (1)$$

The sub-model of the stator voltage (sd₂–sq₂) is expressed as:

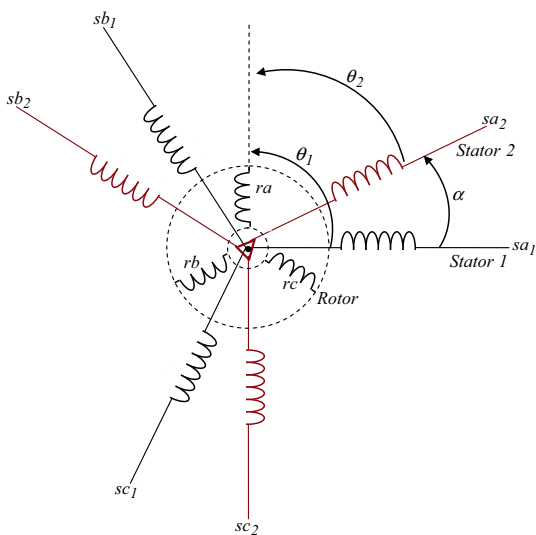


Fig. 1 Structure of the DSIM windings

$$\begin{cases} V_{sd_2} = R_s I_{sd_2} + \frac{d\phi_{sd_2}}{dt} - \omega_s \phi_{sq_2} \\ V_{sq_2} = R_s I_{sq_2} + \frac{d\phi_{sq_2}}{dt} + \omega_s \phi_{sd_2} \end{cases} \quad (2)$$

The sub-model of the rotor voltage (rd–rq) is expressed as:

$$\begin{cases} V_{rd} = 0 = R_r I_{rd} + \frac{d\phi_{rd}}{dt} - \omega_r \phi_{rq} \\ V_{rq} = 0 = R_r I_{rq} + \frac{d\phi_{rq}}{dt} + \omega_r \phi_{rd} \end{cases} \quad (3)$$

The equations of the flux can be expressed as:

$$\begin{cases} \phi_{sd_1} = L_s I_{sd_1} + L_{ms} I_{sd_2} + M I_{rd} \\ \phi_{sq_1} = L_s I_{sq_1} + L_{ms} I_{sq_2} + M I_{rq} \end{cases} \quad (4)$$

$$\begin{cases} \phi_{sd_2} = L_s I_{sd_2} + L_{ms} I_{sd_1} + M I_{rd} \\ \phi_{sq_2} = L_s I_{sq_2} + L_{ms} I_{sq_1} + M I_{rq} \end{cases} \quad (5)$$

$$\begin{cases} \phi_{rd} = L_r I_{rd} + M(I_{sd_1} + I_{sd_2}) \\ \phi_{rq} = L_r I_{rq} + M(I_{sq_1} + I_{sq_2}) \end{cases} \quad (6)$$

The electromagnetic torque is expressed as:

$$T_e = p \frac{M}{L_r} [\phi_{rd}(I_{sq_1} + I_{sq_2}) - \phi_{rq}(I_{sd_1} + I_{sd_2})] \quad (7)$$

In this study, the traditional homopolar components are neglected due to the isolation of the two star’s neutrals. The DSIM voltage equations given in (1)–(3) are similar to those of two separate three-phase machines. Consequently, the DSIM can be controlled in a similar way as in the case of a three-phase machine.

4 Drive control

The control strategy presented in this work allows the tracking of the drive operating point to ensure optimal operating conditions. This approach is based on the indirect rotor flux-oriented control (IRFOC) principle depicted in Fig. 2. In this section, the IRFOC technique applied to the DSIM is firstly presented and then the proposed control strategy is detailed.

The rotor flux components are controlled to fulfill the following conditions:

$$\begin{cases} \phi_{rq} = 0 \\ \phi_{rd} = \phi_r \end{cases} \quad (8)$$

The control of the DSIM is ensured by the stator current components. So, substituting (8) into (6) and eliminating the rotor’s current components from (4) and (5) lead to the following flux expressions:

online to minimize the magnetizing energy, which leads to Joule losses reduction.

In an induction motor, the Joule losses are the sum of the stator P_{js} and rotor P_{jr} losses. Their respective terms are:

$$P_j = P_{js} + P_{jr} \tag{16}$$

As the stator is composed of two identical winding sets, the stator Joule losses become:

$$P_{js} = P_{js_1} + P_{js_2} \tag{17}$$

$$P_{js} = R_s(I_{s_1}^2 + I_{s_2}^2) = R_s[(I_{sd_1}^2 + I_{sq_1}^2) + (I_{sd_2}^2 + I_{sq_2}^2)] \tag{18}$$

Similarly, the Joule losses of the rotor can be expressed as:

$$P_{jr} = R_r I_r^2 = R_r(I_{rd}^2 + I_{rq}^2) \tag{19}$$

By taking into account the steady-state operation with the conditions expressed in (8), and according to (3) and (11), the components of the rotor current become:

$$\begin{cases} I_{rd} = 0 \\ I_{rq} = -\frac{M}{L_r}(I_{sq_1} + I_{sq_2}) \end{cases} \tag{20}$$

Hence, the rotor Joule losses become:

$$P_{jr} = R_r I_{rq}^2 = R_r \left[-\frac{M}{L_r}(I_{sq_1} + I_{sq_2}) \right]^2 \tag{21}$$

Replacing the stator current components by their expressions from (14) and (15) leads to the following Joule losses expression as a function of the electromagnetic torque and magnetic flux:

$$P_j = \frac{R_s}{2M^2} \Phi_r^2 + \frac{1}{p^2} \left[\frac{R_s}{2} \left(\frac{L_r}{M} \right)^2 + R_r \right] \frac{T_e^2}{\Phi_r^2} = k_1 \Phi_r^2 + k_2 \frac{T_e^2}{\Phi_r^2} \tag{22}$$

where

$$k_1 = \frac{R_s}{2M^2}; \quad k_2 = \frac{1}{p^2} \left[\frac{R_s}{2} \left(\frac{L_r}{M} \right)^2 + R_r \right]$$

In order to determine the optimal motor flux which ensures minimum losses, the derivative of (22) leads to:

$$\frac{\partial P_j}{\partial \Phi_r} = 0 = 2k_1 \Phi_r - 2k_2 \frac{T_e^2}{\Phi_r^3} \tag{23}$$

So, the optimal value of Φ_r is as follows:

$$\Phi_{r_opt} = k \sqrt{|T_e|} \tag{24}$$

where $k = \sqrt[4]{\frac{k_2}{k_1}}$.

Expression (24) demonstrates that the magnetic flux is a function of the motor torque, which means that the excitation should be linked to the torque demand. So, the priority of the control is not to minimize losses, but to deliver a magnetic flux according to the desired torque. However, as the operating point of the drive is variable and the value of the nominal flux is considered optimal at nominal point, this constitutes a degree of freedom to minimize the magnetizing power and to reduce the total motor current.

The optimal flux Φ_{r_opt} varies between a minimum value Φ_{r_min} and a maximum value $\Phi_{r_max} = \Phi_{r_nom}$, according to [17]. Through the experimental tests carried out during this work, the minimum value of the flux necessary to ensure the magnetization of the machine is equal to 20% of the nominal flux, so $\Phi_{r_min} = 20\% \Phi_{r_nom}$. As a result, the optimal flux is defined in a range of variation as follows:

$$\Phi_{r_min} \leq \Phi_{r_opt} \leq \Phi_{r_nom}$$

6 Simulation results

Simulations are provided to show the effectiveness of the proposed optimization method. Thus, some tests are performed and compared under IRFOC scheme for both cases, with conventional IRFOC and with the proposed operating point tracking strategy. So, a set of tests are conducted under various light loads and speed conditions, and only two-test cases are reported in this paper.

Hence, in this section simulation results for operating speed fixed firstly at $\Omega = 40$ rad/s and then at $\Omega = 60$ rad/s for different load torques of $T_L = 3$ N m and $T_L = 5$ N m are presented.

Figures 3 and 4 present the simulation results where the motor is initially running at a rotating speed of 40 rad/s under a load torque of 3 N m and then a load torque of

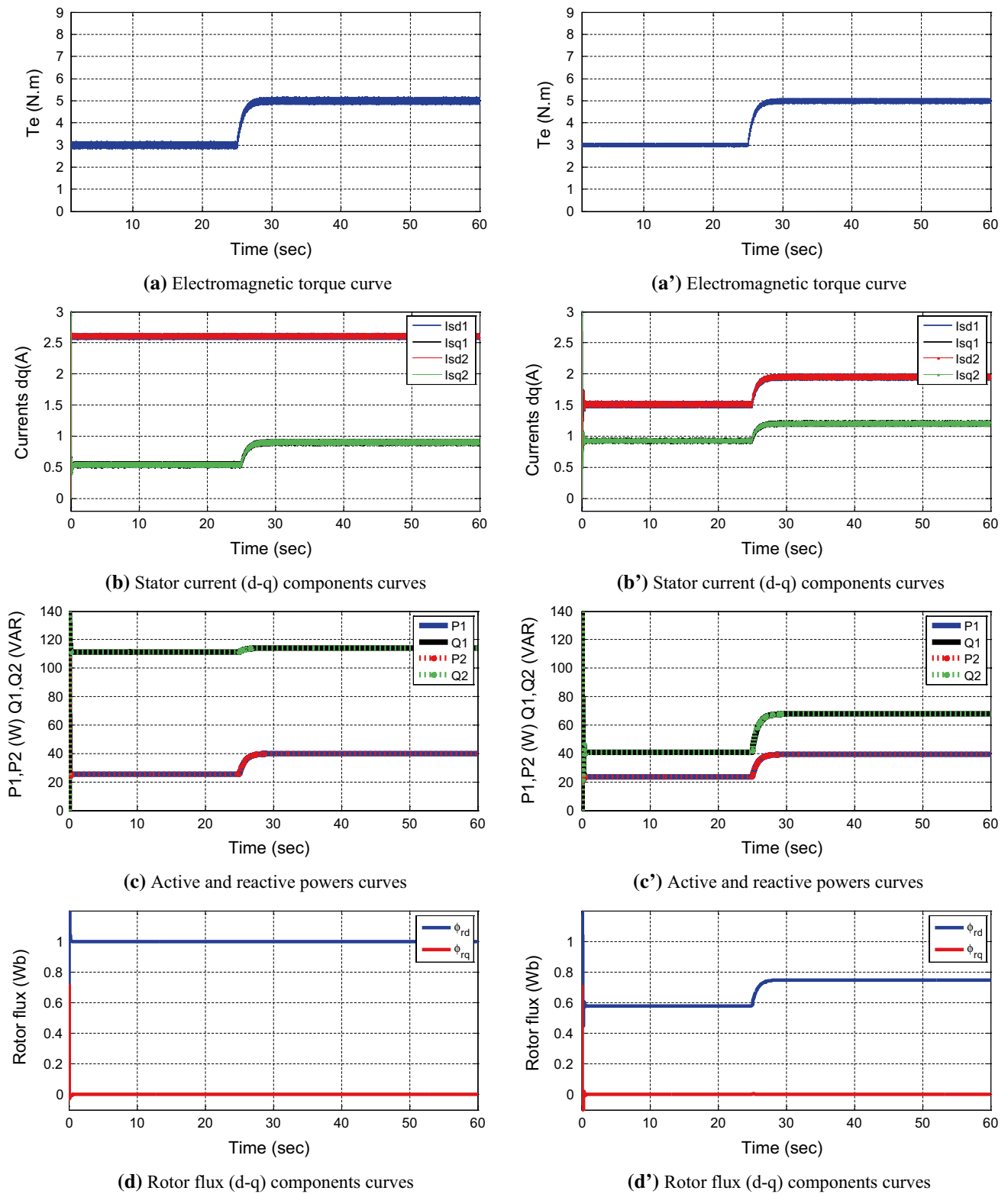


Fig. 3 Simulation results at operating speed of 40 rad/s under a load torque step from 3 to 5 N m: with the proposed operating point tracking strategy (right curves) and with the conventional IRFOC (left curves)

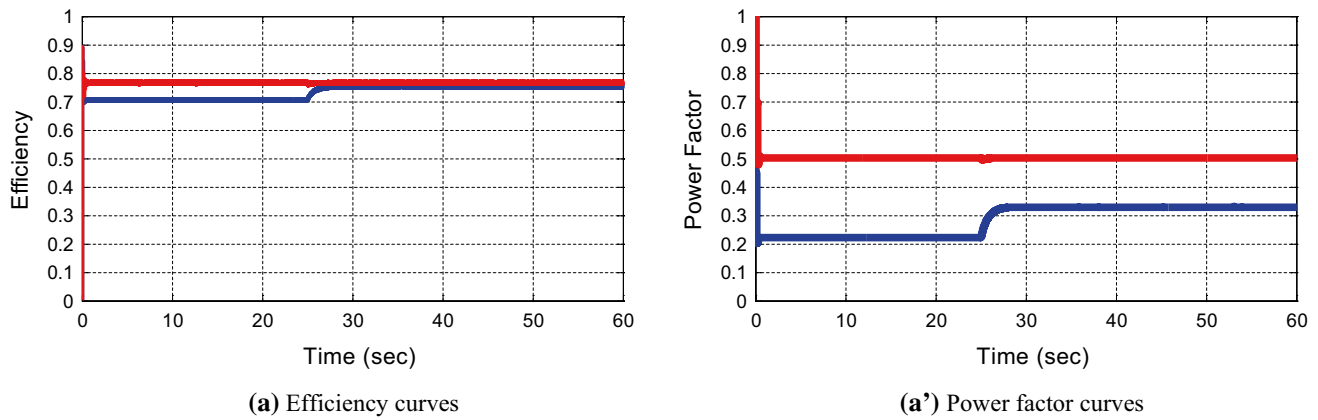


Fig. 4 Simulation results of efficiency and power factor at 40 rad/s under a load torque step from 3 to 5 N m: with the proposed operating point tracking strategy (red curves) and with the conventional IRFOC (blue curves) (color figure online)

Table 1 Simulation values of motor variables at an operating speed of 40 rad/s

Motor variables	Classical IRFOC results		Optimal flux IRFOC (proposed method) results	
	$T_L=3\text{ N m}$	$T_L=5\text{ N m}$	$T_L=3\text{ N m}$	$T_L=5\text{ N m}$
I_{sd1}, I_{sd2} (A)	2.6	2.6	1.5	1.95
I_{sq1}, I_{sq2} (A)	0.55	0.9	0.9	1.2
$I_{s_{abc1}}, I_{s_{abc2}}$ (A)	2.1	2.3	1.45	1.85
P_1, P_2 (W)	25.3	39.8	23.5	39.4
Q_1, Q_2 (VAR)	111.45	114.2	40.5	68
φ_{rd} (Wb)	01	01	0.58	0.75
φ_{rq} (Wb)	00	00	00	00
Joule losses (W)	32	39	21.5	36
Power factor	0.22	0.33	0.5	0.5
Efficiency	0.7	0.76	0.77	0.78

5 N m is applied at the instant $t=25$ s. Also, the main motor variable values under both strategies, in this case, are summarized in Table 1 for comparison purpose.

The presented simulation results show that the rotor flux component φ_{rd} is maintained constant and equals 1 Wb in case of the conventional IRFOC technique, whereas the use of the operating point tracking strategy (proposed strategy) allows a reduction in the rotor flux component

φ_{rd} from 1 to 0.58 Wb (reduction of 42%) in case of a load torque of 3 N m and from 1 to 0.75 Wb (reduction of 25%) in case of a load torque of 5 N m, as shown in Fig. 3d, d'. The reduction in the rotor flux allowed a reduction in the stator currents from 2.1 to 1.45 A (reduction of 31%) in case of a load torque of 3 N m and from 2.3 to 1.85 A (reduction of 19.56%) in case of a load torque of 5 N m, which is demonstrated in Fig. 3b, b', where a reduction in the stator current components $I_{sd1,2}$ is clearly shown and confirmed according to the relation $I_{sd} = \frac{\varphi_r}{M}$ derived from Eq. (14). However, a slight increase in the stator current components $I_{sq1,2}$ is observed in Fig. 3b, b', and this can be explained using the relation $I_{sq} = \frac{L_r C_e}{p \cdot M \cdot \varphi_r}$ derived from Eq. (15). Also, a reduction in the reactive power from 111.45 to 40.5 VAR (reduction of 63.66%) in case of a load torque of 3 N m and from 114.2 to 68 VAR (reduction of 40.45%) in case of a load torque of 5 N m is shown in Fig. 3c, c', which leads to the optimization of reactive energy needed to machine magnetization, and consequently, a significant improvement in the power factor from 0.22 to 0.5 (enhancement of 56%) in case of a load torque of 3 N m and from 0.33 to 0.5 (enhancement of 34%) in case of a load torque of 5 N m is realized as shown in Fig. 4a'.

Figure 4a presents the efficiency curves and shows that the efficiency obtained at light load using the proposed control strategy is better compared to the conventional

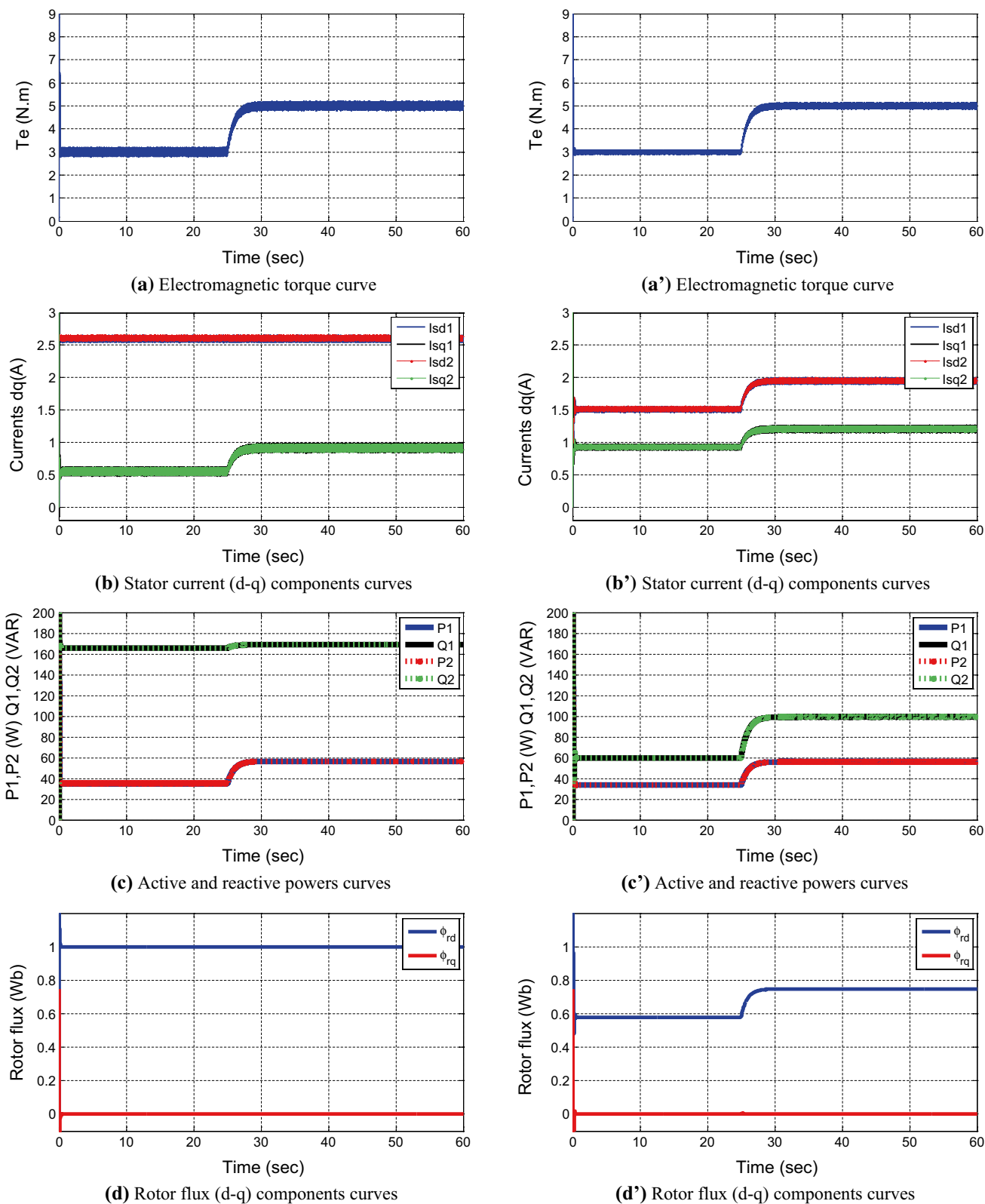


Fig. 5 Simulation results at an operating speed of 60 rad/s under a load torque step from 3 to 5 N.m: with the proposed operating point tracking strategy (right curves) and with the conventional IRFOC (left curves)

Table 2 Simulation values of motor variables at an operating speed of 60 rad/s

Motor variables	Classical IRFOC results		Optimal flux IRFOC (proposed method) results	
	$T_L=3\text{ N m}$	$T_L=5\text{ N m}$	$T_L=3\text{ N m}$	$T_L=5\text{ N m}$
I_{sd1}, I_{sd2} (A)	2.60	2.60	1.50	1.95
I_{sq1}, I_{sq2} (A)	0.55	0.90	0.92	1.20
$I_{s_{abc1}}, I_{s_{abc2}}$ (A)	2.1	2.3	1.45	1.9
P_1, P_2 (W)	35	56.5	33.6	56
Q_1, Q_2 (VAR)	166	169	59.6	99.5
φ_{rd} (Wb)	01	01	0.58	0.75
φ_{rq} (Wb)	00	00	00	00
Joule losses (W)	32	40	22	36
Power factor	0.21	0.32	0.49	0.49
Efficiency	0.77	0.81	0.82	0.83

IRFOC technique. So, an improvement in the efficiency from 70 to 77% in case of a load torque of 3 N m and from 76 to 78% in case of a load torque of 5 N m is reached as shown in Fig. 4a.

The simulation results under an operating speed of $\Omega = 60$ rad/s under load torques of $T_L = 3$ N m and $T_L = 5$ N m are presented in Fig. 5, and the main motor variable values under both strategies are summarized in Table 2. Also, the simulation results conducted under an operating speed of $\Omega = 60$ rad/s show that the proposed method always gives better performances with a slight influence of the speed on the results as shown in Figs. 5 and 6 and summarized in Table 2.

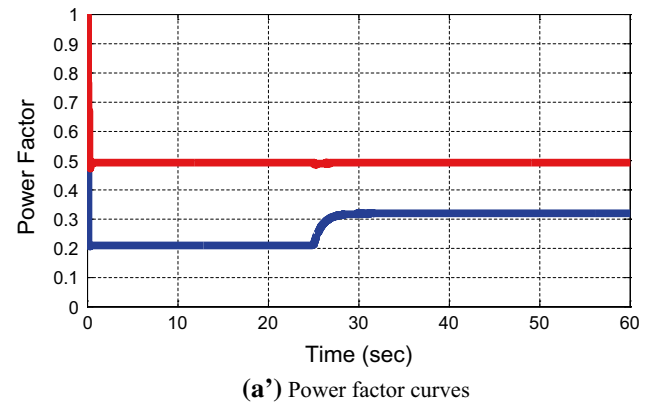
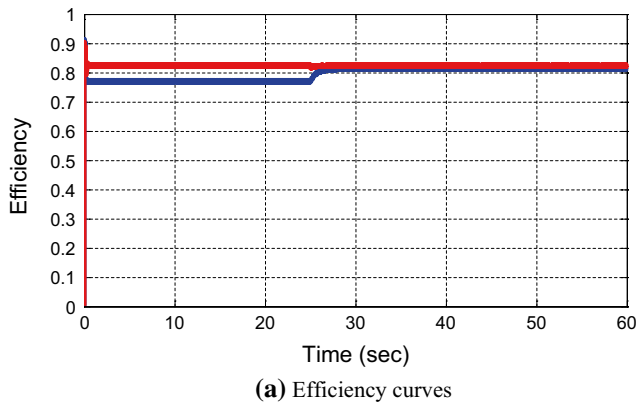
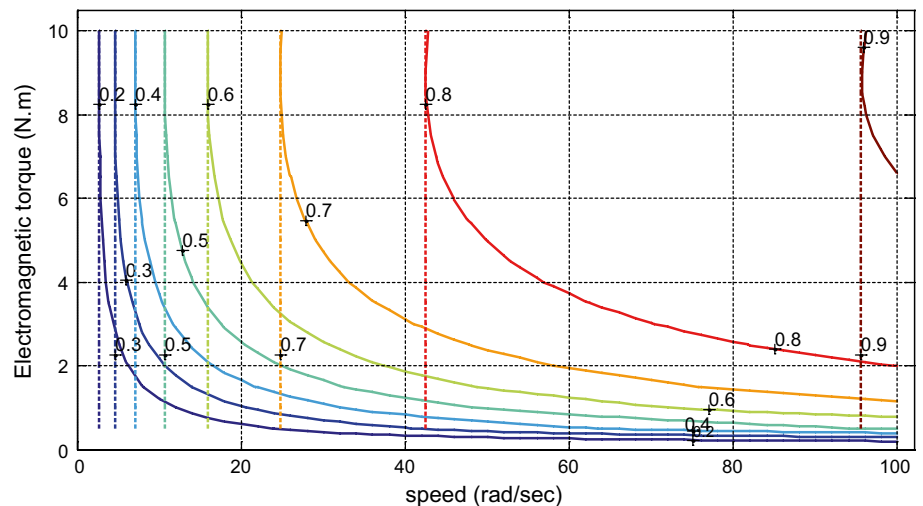


Fig. 6 Simulation results of efficiency and power factor at 60 rad/s under a load torque step from 3 to 5 N m: with the proposed operating point tracking strategy (red curves) and with the conventional IRFOC (blue curves) (color figure online)

Fig. 7 Efficiency map in the torque–speed plan: with the operating point tracking strategy (dashed lines) and with conventional IRFOC (continuous lines)



7 Efficiency evaluation

This section gives a comparison of motor efficiency map of both control techniques for more details. So, the motor efficiency is evaluated using the following usual expression:

$$\eta = \frac{P_u}{P_u + P_{\text{losses}}} \quad (25)$$

where P_u is the motor mechanical output power and P_{losses} is the total power losses. If the mechanical losses are neglected, the output power can be expressed as a function of the electromagnetic torque and the rotational speed as follows:

$$P_u = T_e \cdot \Omega \quad (26)$$

Replacing the Joule losses by (22), the efficiency expression can be rewritten as follows:

$$\eta = \frac{\Omega \cdot T_e}{\Omega \cdot T_e + k_1 \Phi_r^2 + k_2 \frac{T_e^2}{\Phi_r^2}} \quad (27)$$

Substituting the rotor flux into (24) leads to the optimal efficiency expression given as:

$$\eta_{\text{opt}} = \frac{\Omega}{\Omega + k_1 k^2 + \frac{k_2}{k^2}} \quad (28)$$

The efficiency map including several speed and load points is plotted in a single torque–speed plan using the developed efficiency analytical expressions (27) and (28) for the conventional IRFOC and the operating point tracking strategy (proposed method), respectively. Hence, Fig. 7 shows that for a given speed, the efficiency is load dependent and increases as a function of this load to reach an optimal value. On the other hand, with the proposed method the efficiency optimal value is reached whatever the load according to (28). Also, the efficiency trajectories for both strategies become superposed when the rotor flux reaches its nominal value. Evidently, it is clear that these analytical results coincide with those of simulation (Figs. 4a, 6a) as well as experiments (Figs. 10a, 12a of the experimental section), which reinforces this study.

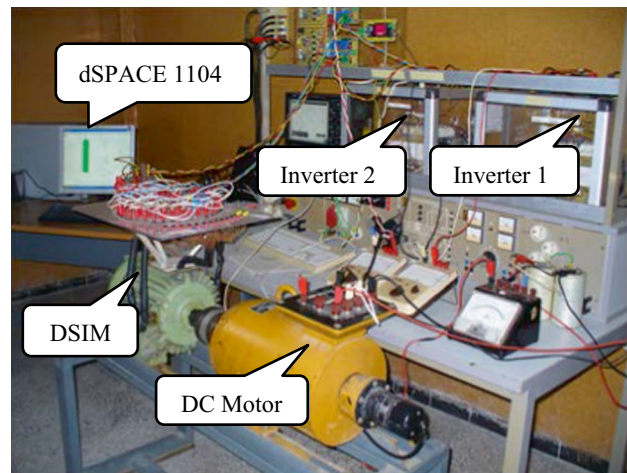


Fig. 8 Photography of the experimental test bench

8 Experimental results

Experimental tests have been carried out on the test bench shown in Fig. 8. The test bench is composed of a prototype of DSIM (5.5 kW, six poles), whose parameters are given in “Appendix,” a DC machine used as a load, a two three-phase VSI feeding the machine and a dSPACE DS1104 controller board which is used to control the overall system.

The experimental tests are carried out under the same conditions as numerical simulations provided previously (at operating speeds of 40 and 60 rad/s at light loads $T_L = 3 \text{ N m}$ and $T_L = 5 \text{ N m}$).

Figures 9 and 10 show the experimental results corresponding to operating speed of 40 rad/s, and the main variable values are summarized in Table 3. According to these results, the proposed strategy allowed a reduction in the rotor flux to 0.57 Wb (reduction of 43%) and to 0.74 Wb (reduction of 26%) in case of a load torque of 3 N m and 5 N m, respectively, as shown in Fig. 9d'. So, a reduction in the d-current component from 2.5 to 1.4 A (reduction of 44%) and from 2.5 to 1.85 A (reduction of 26%) in case of a load torque of 3 N m and 5 N m, respectively, is clearly shown in Fig. 9b, b'. Therefore, an optimization of the reactive power

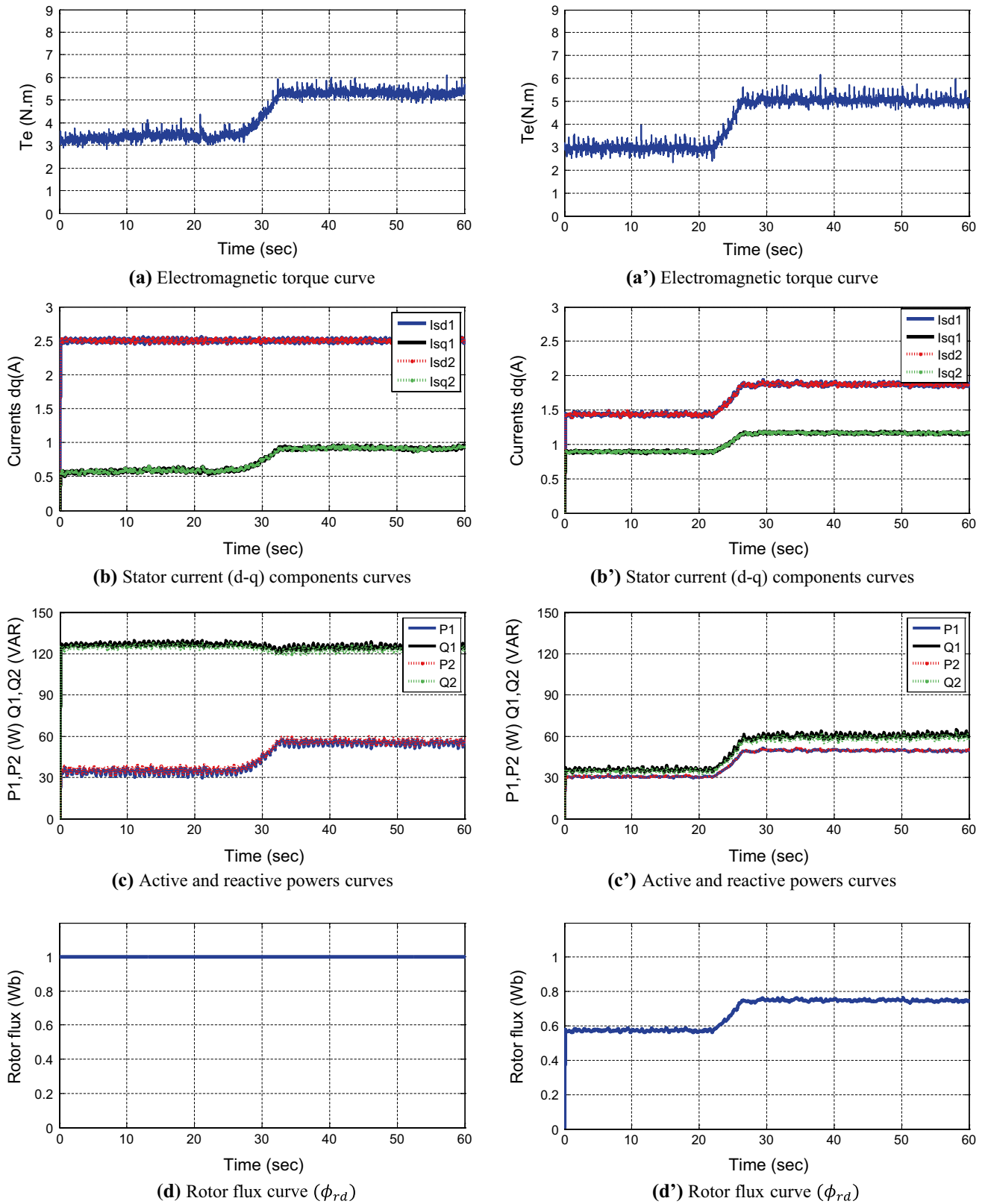


Fig. 9 Experimental results at an operating speed of 40 rad/s under a load torque step from 3 to 5 N m: with the proposed operating point tracking strategy (right curves) and with the conventional IRFOC (left curves)

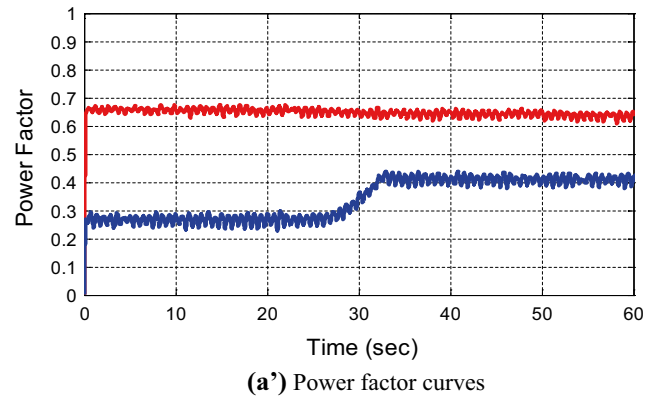
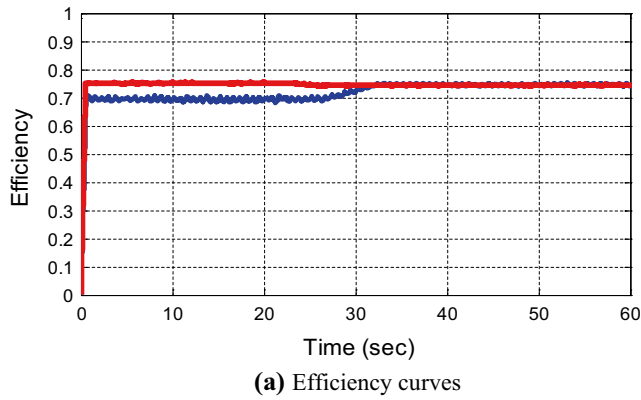


Fig. 10 Experimental results of efficiency and power factor at 40 rad/s under a load torque step from 3 to 5 N m: with the proposed operating point tracking strategy (red curves) and with the conventional IRFOC (blue curves) (color figure online)

Table 3 Experimental values of motor variables at an operating speed of 40 rad/s

Motor variables	Classical IRFOC results		Optimal flux IRFOC (proposed method) results	
	$T_L = 3 \text{ N m}$	$T_L = 5 \text{ N m}$	$T_L = 3 \text{ N m}$	$T_L = 5 \text{ N m}$
I_{sd1}, I_{sd2} (A)	2.5	2.5	1.4	1.85
I_{sq1}, I_{sq2} (A)	0.56	0.92	0.85	1.16
$I_{s_{abc1}}, I_{s_{abc2}}$ (A)	2.0	2.2	1.3	1.7
P_1, P_2 (W)	35	56	30	50
Q_1, Q_2 (VAR)	126	124	35	60
φ_{rd} (Wb)	01	01	0.57	0.74
φ_{rq} (Wb)	00	00	00	00
Joule losses (W)	30.5	37	20.5	34
Power factor	0.27	0.40	0.66	0.64
Efficiency	0.69	0.74	0.75	0.76

from 126 to 35 VAR (reduction of 72.22%) and from 124 to 60 VAR (reduction of 51.61%) is obtained, as shown in Fig. 9c, c'. The optimization of reactive power leads to a significant improvement in the power factor from 0.27 to 0.66 (enhancement of 59.09%) and from 0.40 to 0.64 (enhancement of 37.5%) in case of a load torques of 3 N m and 5 N m, respectively, as shown in Fig. 10a'.

Figure 10a presents the efficiency curves, and using the proposed control strategy, an improvement in the efficiency from 69 to 75% in case of a load torque of 3 N m and from 74 to 76% in case of a load torque of 5 N m is reached as shown in Fig. 10a.

Also, the experimental results under an operating speed of $\Omega = 60 \text{ rad/s}$ under load torques of $T_L = 3 \text{ N m}$ and $T_L = 5 \text{ N m}$ are presented in Fig. 11, and the main motor variable values under both strategies are summarized in Table 4. These experimental results show that the proposed method always gives better performances with a slight influence of the speed as shown in Figs. 11 and 12 and summarized in Table 4.

The obtained experimental results are very close to those of the simulation and confirm all the conclusions about the improvements in the efficiency and power factor of drive system under light-load conditions, by calculating and adjusting the rotor flux optimal reference according to the operating point.

9 Conclusion

In this paper, a novel losses minimization strategy to enhance the efficiency and power factor of a DSIM drive system is proposed. The main idea of the proposed strategy is to select optimal rotor flux reference, which ensures motor

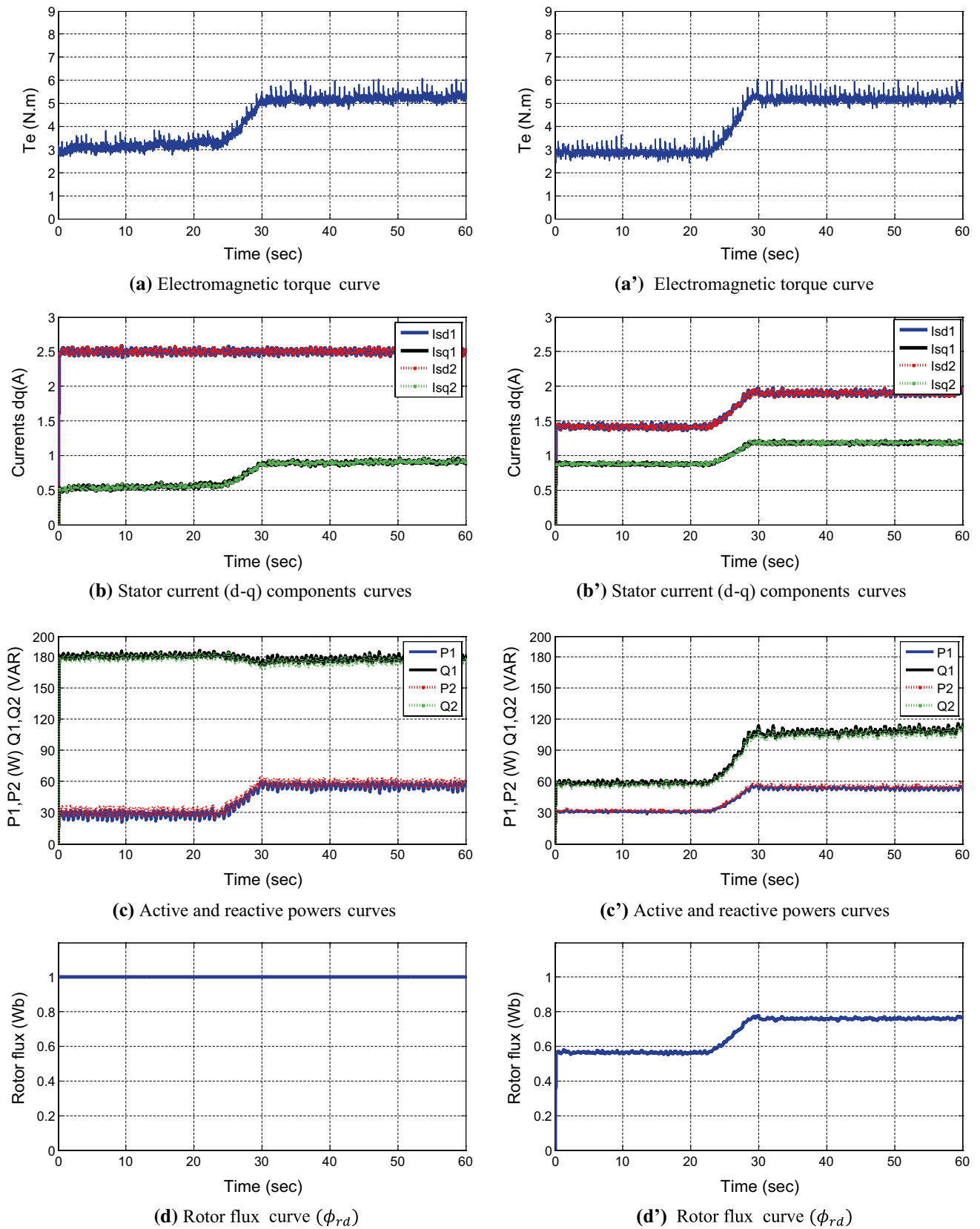


Fig. 11 Experimental results at an operating speed of 60 rad/s under a load torque step from 3 to 5 N m: with the proposed operating point tracking strategy (right curves) and with the conventional IRFOC (left curves)

Table 4 Experimental values of motor variables at an operating speed of 60 rad/s

Motor variables	Classical IRFOC results		Optimal flux IRFOC (proposed method) results	
	$T_L=3\text{ N m}$	$T_L=5\text{ N m}$	$T_L=3\text{ N m}$	$T_L=5\text{ N m}$
I_{sd1}, I_{sd2} (A)	2.50	2.50	1.44	1.9
I_{sq1}, I_{sq2} (A)	0.55	0.90	0.88	1.18
$I_{s_{abc1}}, I_{s_{abc2}}$ (A)	2.0	2.3	1.35	1.7
P_1, P_2 (W)	30	57	31	54
Q_1, Q_2 (VAR)	180	175	57	105
φ_{rd} (Wb)	01	01	0.55	0.76
φ_{rq} (Wb)	00	00	00	00
Joule losses (W)	30.2	37.5	19.5	35.5
Power factor	0.19	0.31	0.48	0.46
Efficiency	0.74	0.83	0.83	0.84

losses reduction. The rotor flux reference is calculated online according to the drive operating point, especially under light-load conditions.

Simulation and experimental results confirm that by adjusting the motor’s magnetic state, according to the drive operating point, the magnetizing energy is reduced allowing a reduction in the current circulating through the motor windings, which leads to copper losses reduction and therefore to machine efficiency and power factor improvement.

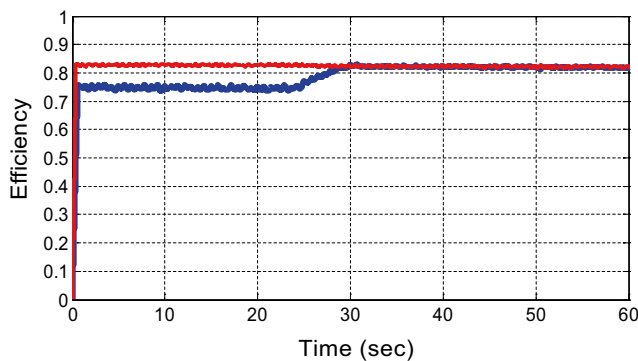
Besides, in high-power applications, reduced copper losses are important to maintain thermal limits, which participate in the cooling system optimization and hence in the improvement in the total energy efficiency of the drive system.

Appendix

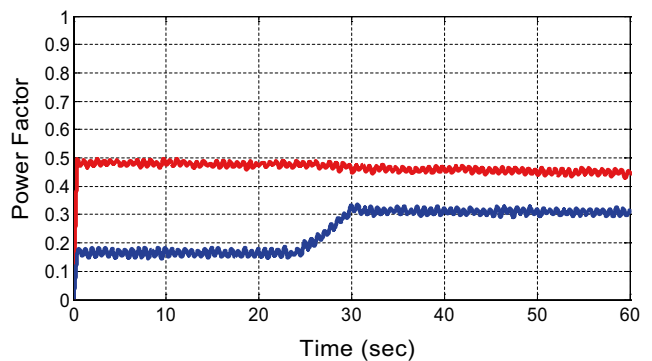
See Table 5.

Table 5 Dual star induction machine parameters

Quantity	Symbol and magnitude
Rated power	$P_n=5.5\text{ kW}$
Rated voltage	$V_n=110\text{ V}$
Rated current	$I_n=6\text{ A}$
Rated speed	$N_n=950\text{ rpm}$
Number of poles	$2 * p=6$
Rated Frequency	$f=50\text{ Hz}$
Stator resistance	$R_s=2.03\ \Omega$
Rotor resistance	$R_r=3\ \Omega$
Stator inductance	$L_s=0.215\text{ H}$
Rotor inductance	$L_r=0.215\text{ H}$
Mutual inductance	$M=0.2\text{ H}$
Moment of inertia	$J=0.06\text{ kg m}^2$
Coefficient of viscous friction	$k_f=0.006\text{ N m s/rad}$



(a) Efficiency curves



(a') Power factor curves

Fig. 12 Experimental results of efficiency and power factor at 60 rad/s under a load torque step from 3 to 5 N m: with the proposed operating point tracking strategy (red curves) and with the conventional IRFOC (blue curves) (color figure online)

References

1. Levi E (2008) Multiphase electric machines for variable-speed applications. *IEEE Trans Ind Electron* 55(5):1893–1909
2. Barrero F, Duran MJ (2016) Recent advances in the design, modeling, and control of multiphase machines part I. *IEEE Trans Ind Electron* 63(1):449–458
3. Duran MJ, Barrero F (2016) Recent advances in the design, modeling, and control of multiphase machines part II. *IEEE Trans Ind Electron* 63(1):459–468
4. Marouani K, Nounou K, Benbouzid M, Tabbache B (2018) Investigation of energy-efficiency improvement in an electrical drive system based on multi-winding machines. *Electr Eng* 100(1):205–216
5. Klingshirn EA (1983) High phase order induction motors—part I: description and theoretical consideration. *IEEE Trans Power Appar Syst* 102:47–53
6. Marouani K, Baghli L, Hadiouche D, Kheloui A, Rezzoug A (2008) A new PWM strategy based on a 24-sector vector space decomposition for a six-phase VSI-fed dual stator induction motor. *IEEE Trans Ind Electron* 55(5):1910–1920
7. Melo VFMB, Jacobina CB, Rocha N (2017) Fault tolerance performance of dual-inverter-based six-phase drive system under single-two-, and three-phase open-circuit fault operation. *IET Power Electron* 11(1):212–220
8. Marouani K, Nesri M, Nounou K (2016) Rotor flux control with copper losses reduction in a high power drive system. In: *IEEE international power electronics and motion control conference (PEMC'2016)*
9. Negahdari A, Yepes AG, Doval-Gandoy J, Toliyat H (2018) Efficiency enhancement of multiphase electric drives at light-load operation considering both converter and stator copper losses. *IEEE Trans Power Electron* 34:1518–1525
10. Boglietti A, Bojoi R, Cavagnino A, Tenconi A (2008) Efficiency analysis of PWM inverter fed three-phase and dual three-phase high frequency induction machines for low/medium power applications. *IEEE Trans Ind Electron* 55(5):2015–2023
11. Bodo N, Levi E, Subotic L, Espina J, Empringham L, Johnson CM (2017) Efficiency evaluation of fully integrated on-board EV battery chargers with nine-phase machines. *IEEE Trans Energy Convers* 32(1):257266
12. Lai JS, Yu W, Sun P, Leslie S, Arnet B, Smith C, Cogan A (2014) A hybrid-switch-based soft-switching inverter for ultra-high-efficiency traction motor drives. *IEEE Trans Ind Appl* 50(3):1966–1973
13. Lipo TA (1980) A dq model for six phase induction machines. In: *Proceedings of ICEM'80*, pp 860–867
14. Vas P (1998) *Sensorless vector and direct torque control*. Oxford University Press, Oxford
15. Zhao Y, Lipo TA (1995) Space vector PWM control of dual three phase induction machine using vector space decomposition. *IEEE Trans Ind Appl* 31(5):1100–1109
16. Abbas MA, Christen R, Jahns TM (1984) Six-phase voltage source inverter driven induction motor. *IEEE Trans Ind Appl* 5:1251–1259
17. Boukhelifa A (2007) *Optimization elements for controlling an asynchronous machine for vector control*. PhD Thesis, National Polytechnic School, Algiers, Algeria (**in French**)

Publisher's Note Springer Nature remains neutral with regard to jurisdictional claims in published maps and institutional affiliations.